A CLASSIFICATION SCHEME FOR VISUAL DEFECTS ARISING IN SEMICONDUCTOR WAFER INSPECTION

A. Ravishankar RAO *

IBM Thomas J. Watson Research Center, P.O. Box 218, Yorktown Heights, New York 10598-0704, USA

and

Ramesh JAIN

Artificial Intelligence Laboratory, University of Michigan, Ann Arbor, Michigan 48109-2110, USA

In this paper we describe a novel scheme to characterize surface defects and flaws that arise in semiconductor wafer processing. This is done by analyzing the texture of an image of the defect. We have developed a taxonomy for textures, which classifies textures into the broad classes of disordered, strongly ordered and weakly ordered. Disordered textures are described in terms of their fractal dimension, strongly ordered textures are by the placement of primitives, and weakly ordered textures by the underlying orientation field. We have developed an algorithm to measure the fractal dimension of a given texture. We use the qualitative theory of differential equations to devise a symbol set for the weakly ordered textures in terms of singularities. We have devised an algorithm to process an image of a defect and extract qualitative descriptions based on this theory.

1. Introduction

The identification, description and classification of defects and anomalies is a difficult problem in process control and automated inspection. Unfortunately, there is no *standardized* scheme to describe defects and anomalies. Most of the features used are highly subjective, and terminology varies considerably.

Hence, there is a need for designing a standardized description scheme. The advantages of a standardized scheme are that it will allow for a description of new defects that may arise in the future and that cataloging the defects will become systematic [1]. Faced with an absence of standardized symbols, inspection personnel in the semiconductor industry are forced to devise peculiar jargon to describe various textures that are created during the manufacturing process.

Fig. 1 illustrates some concrete jargon that is popularly used to describe different kinds of anomalies and defects arising during wafer processing. Such a scheme is ad-hoc, and a more scientific scheme is desirable.

Texture plays a critical role in inspecting surfaces that are produced at various stages in all types of manufacturing [2]. For instance, in the inspection of semiconductor devices, surface texture is an important factor that is used to decide
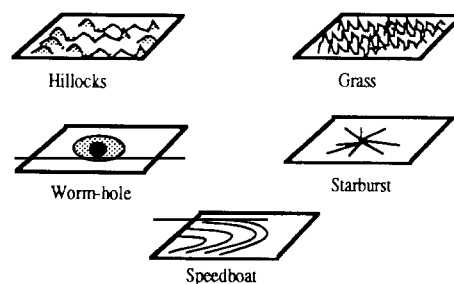

Fig. 1. Illustration of the jargon used by the semiconductor industry to describe different kinds of visual defects arising during the manufacturing process.

* Formerly at the Artificial Intelligence Laboratory, University of Michigan, Ann Arbor, Michigan 48109-2110, USA.

the integrity of a fabricated device [3]. Since many types of defects are rich in textural content, we have devised a standardized taxonomy to classify and describe textural defects.

1.1. The proposed classification scheme

Fig. 2 shows the proposed scheme, which is hierarchically ordered. Textures are broadly divided into ordered and disordered textures, based on the presence of repetitive primitive elements and the directionality of the texture. Textures having neither directionality nor repetitiveness are called disordered, e.g. sand. Textures that exhibit repetition of some primitive element are called strongly ordered, e.g. brick wall, honeycomb. Textures that exhibit directionality (which may vary locally) but do not contain a primitive element are called weakly ordered, or flow-like, e.g., wood grains, fractographs.

2. Analyzing disordered textures

In order to analyze disordered textures, we need to describe parameters related to the roughness of the texture. For the measurement of roughness we have implemented an algorithm to compute the fractal dimension of a surface, called the "reticular cell counting" approach [4]. The fractal dimension of the texture consititutes a useful measure of roughness. This is because studies have shown [5] the fractal dimension to correlate very well with a human's assessment of surface

roughness. The fractal dimension defines how jagged or crumpled a surface is, $D = 2$ corresponding to a flat plane and $D = 3$ corresponding to a highly spiked surface.

This method has been implemented [6], and the results of applying the method to some IC images are shown in figs. 3a through 3d. The boxes in the image show the regions selected for roughness measurement. The numbers within the boxes show the fractal dimension computed for that part of the image.

3. Analyzing weakly ordered textures

Weakly ordered, or oriented textures are characterized by local selectivity of orientation, which can vary arbitrarily over the entire image. In other words, the texture is anisotropic. Every point in the image is associated with a dominant local orientation, and a local measure of the coherence or degree of anisotropy of the flow pattern. We define the orientation field of a texture image to be comprised of two images, called the angle image and coherence image. The angle image captures the dominant local orientation at each point in the texture in terms of an angle, and the coherence image represents the degree of anisotropy at each point in the texture.

3.1. Overview of approach

Our approach to the problem of oriented texture description is to view it as a two-stage process. The first stage is concerned with extracting
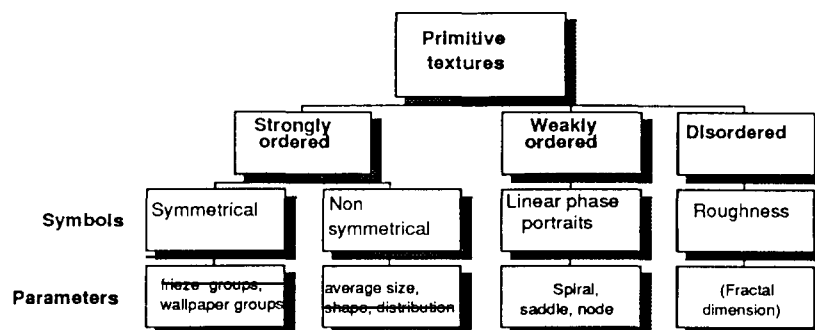

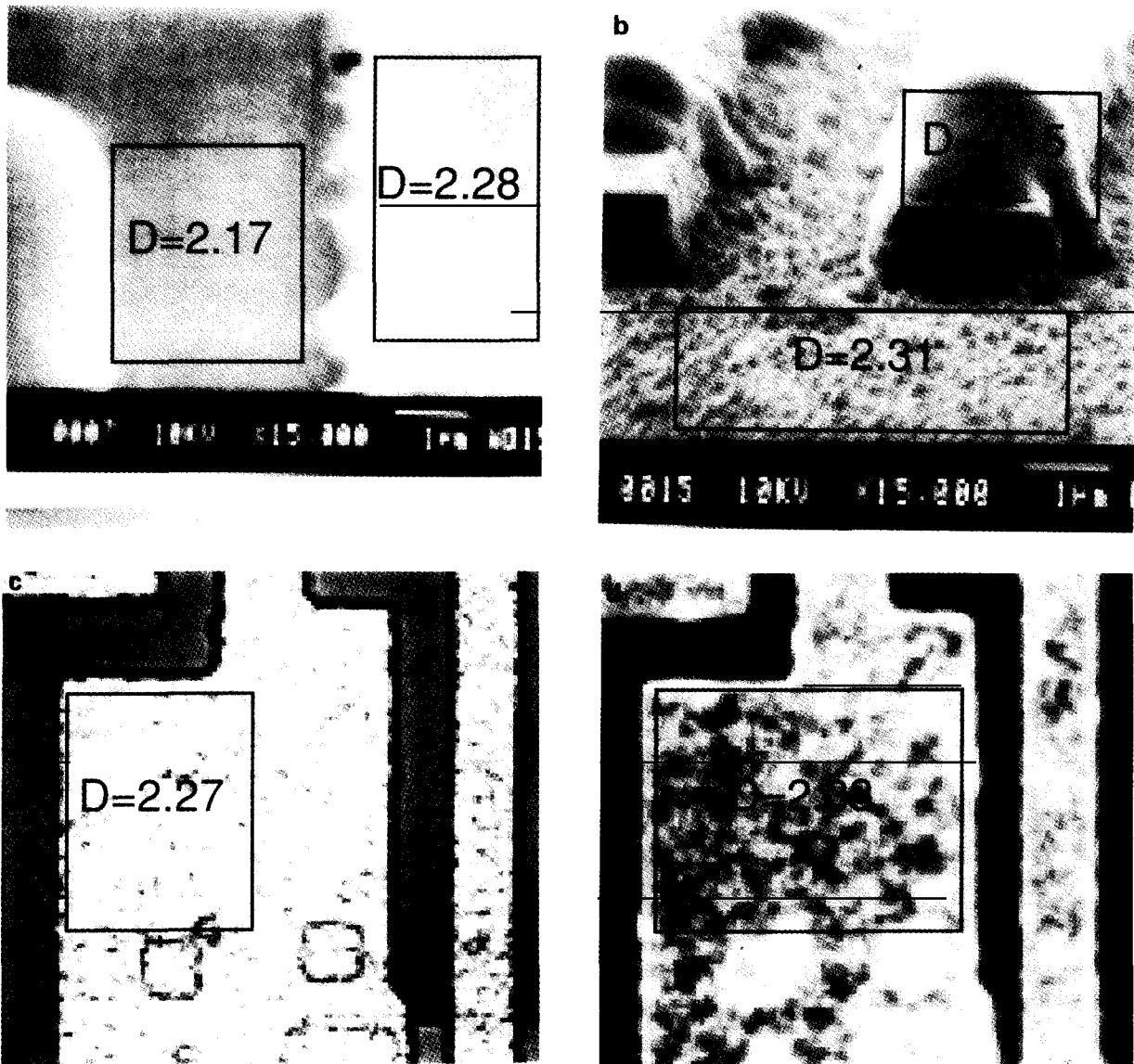Fig. 2. Illustration of the taxonomy for texture.

Fig. 3. The results for surface roughness measurement using fractal dimension. (a) SEM image of a silicon wafer. The surface on the right is rougher than the surface on the left. hence the fractal dimension for the right surface is higher than that of the left surface. This result shows that the fractal dimension corresponds to the intuitive ordering of surface roughness. (b) SEM image of a GaAs wafer. The surface consists of metal deposited via evaporation on a substrate after an RIE etch process. (c) Image of a silicon wafer obtained through an optical microscope. (d) Dark field image of a silicon wafer.

an orientation field from the raw image. We use the algorithm developed by Rao and Schunck [7] in order to extract the orientation field.

The second stage is concerned with performing computations on the orientation field in order to derive a qualitative description. This is described in section 4.

3.2. Obtaining the orientation field

We present a brief overview of the method for estimating the orientation of a texture field, and details may be found in ref. [7].

There are five steps to estimating the local orientation of the texture field:

(1) smooth the image with a Gaussian filter tuned to the wavelength of the pattern;

(2) compute the gradient of the smoothed image;

(3) find the local orientation angle;

(4) average the local orientation estimates over a small neighborhood;

(5) compute a measure of the coherence (the degree of flow-like texture) of the pattern.

The *coherence* of the oriented texture pattern is a measure for how strongly anisotropic the texture is within a local neighborhood. Let the gradient vector at point (i, j) in the image have the polar representation $G_{ij}e^{i\theta_{ij}}$. Thus, the estimate of the dominant orientation $\hat{\theta}$ at the center (m, n) of an $N \times N$ neighborhood of the image is given by

$$\hat{\theta}_{mn} = \frac{1}{2} \tan^{-1} \left(\frac{\displaystyle\sum_{i=m-N/2}^{i=m+N/2} \sum_{j=n-N/2}^{j=n+N/2} G_{ij}^2 \sin 2\theta_{ij}}{\displaystyle\sum_{i=m-N/2}^{i=m+N/2} \sum_{j=n-N/2}^{j=n+N/2} G_{ij}^2 \cos 2\theta_{ij}} \right).$$

(1)

The estimated orientation angle at (m, n) is then $\hat{\theta}_{mn} + \pi/2$, since the gradient vector is perpendicular to the direction of anisotropy. Let $\hat{\theta}_{mn}$ denote the estimated orientation angle at point (m, n), found in the earlier step. To find the coherence at point (m, n), consider the point (i, j), where i and j are chosen so that they fall within a window W of prescribed size around the point (m, n). The measure of coherence is defined by

$$\rho = G_{mn} \frac{\displaystyle\sum_{(i,j)\in W} \| G_{ij} \cos(\hat{\theta}_{ij} - \hat{\theta}_{mn}) \|}{\displaystyle\sum_{(i,j)\in W} G_{ij}}.$$

(2)

Thus, one can obtain a description of the texture by using eqs. (1) and (2).

3.3. Analyzing an orange peel defect

An *orange peel* defect arises when the surface texture appears wrinkled, like the skin of an orange. Such a wrinkled texture is actually an oriented texture, and the method described in this section can be used.

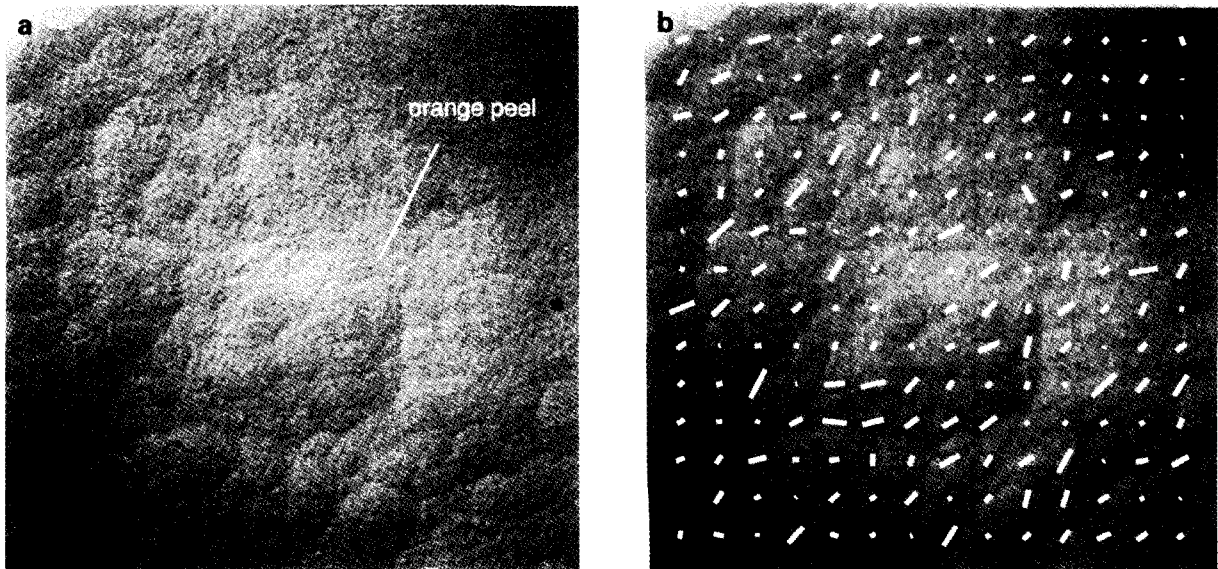Fig. 4a shows an image of an orange peel defect. The sample consists of a silicon wafer that

Fig. 4. (a) The original image of the orange peel defect, obtained at a magnification of 500, using Nomarski phase contrast. (b) The orientation field overlayed on the original image in the form of white segments.

has undergone an isotropic etch using hydrofluoric and nitric acids. The photoresist has a wrinkled appearance, and the appropriate classification for this type of defect is to term it a weakly ordered texture. Fig. 4b shows the orientation field overlayed on the original image. The orientation field is portrayed by white segments, such that the direction of the segment corresponds to the orientation of the underlying texture, and the length of the segment is proportional to the coherence of the texture.

Currently, inspection technicians use terms like "moderate" orange peel and "severe" orange peel to describe the severity of the defect. However, no precise quantitative measure is available. Hence, we propose the following measure for the severity of an oriented texture defect, such as orange peel. Find the average coherence $\bar{\rho}$ over the image of the defect, where ρ is defined in (2).

In the case of the image shown in fig. 4, the average coherence measure for the region of orange peel is 0.12, which represents the severity of the defect.

4. Using phase portraits to analyze the orientation field

The question that we address in this section is: *given the orientation field, what higher level (symbolic) descriptors of the field are meaningful?* This will provide qualitative descriptions of the texture.

The problem is formulated with the help of concepts from the geometric approach to differential equations. The basic idea is to view a given texture flow pattern as being comprised of piecewise linear flows, and to describe each linear flow by means of an equivalent phase portrait. The phase portrait is a two-dimensional figure and represents the qualitative behaviour of a system of differential equations by a family of trajectories.

A system

$$\dot{x}(t) = \frac{dx}{dt} = X(x),\tag{3}$$

where x is a vector in R^n is called a *linear system* of dimension n if $X: R^n \to R^n$ is a linear mapping. It can be shown that only a finite number of

qualitatively different phase portraits can arise for linear systems [8]. If $X: R^n \to R^n$ is a linear mapping, eq. (3) can be written in the form

$$\dot{x}(t) = X(x) = Ax,\tag{4}$$

where A is the coefficient matrix.

To examine the qualitative behavior in the plane, we must look at the *fixed points* or *singular points* of eq. (3). When matrix A is non-singular, we get the phase portraits summarized in fig. 7. The phase portraits are shown in a neighborhood of the origin, which is the fixed point. The nomenclature for the types of phase portrait, viz. *node, saddle; star-node, improper node, center* and *spiral* are standard terms in the geometric theory of differential equations [9,8].

In the case of an affine transformation we get

$$\dot{x}(t) = X(x) = Ax + b,\tag{5}$$

where b is a constant vector. The above equation has a fixed point at

$$x_0 = -A^{-1}b.\tag{6}$$

One can treat a texture as being comprised of *piecewise* linear flow. What we must accomplish is to uncover the differential equation, or the phase portrait that best matches a portion of the given texture. This will allow for a qualitative description of the texture which is firmly grounded in the theory of differential equations. The process is discussed in detail in ref. [10].

Segmentation of the flow image into qualitatively different classes can be performed once we obtain an estimate of the form

$$\dot{x}(t) = \hat{A}x + \hat{b},\tag{7}$$

where $\hat{A}$ and $\hat{b}$ are least squares estimates. Least squares fitting is performed over successive overlapping windows of size 11×11 until the entire image is covered. Fixed points can be identified by using eq. (6).

Once the fixed points of various phase portraits are identified, we can find ou the values of matrices $\hat{A}$ and $\hat{b}$ that represent the best fit at each fixed point. This information can be used to reconstruct the given texture within a neighborhood of the fixed point. This is the method we use in order to

reconstruct salient features of the original texture.

To summarize, we obtain a segmentation of the given texture, and the computation of a likelihood map describing the locations of singularities or fixed points. These results are then used to derive symbolic descriptions of the given textures, and to reconstruct the original texture based on these descriptions.

4.1. Analysis of a resist gel defect

Fig. 5a shows a 240 × 240 image of resist center defect, obtained from ref. [11]. The result of applying the orientation estimation algorithm described in section 3.2 is displayed in fig. 5b. The orientation field is calculated for each point in the image,
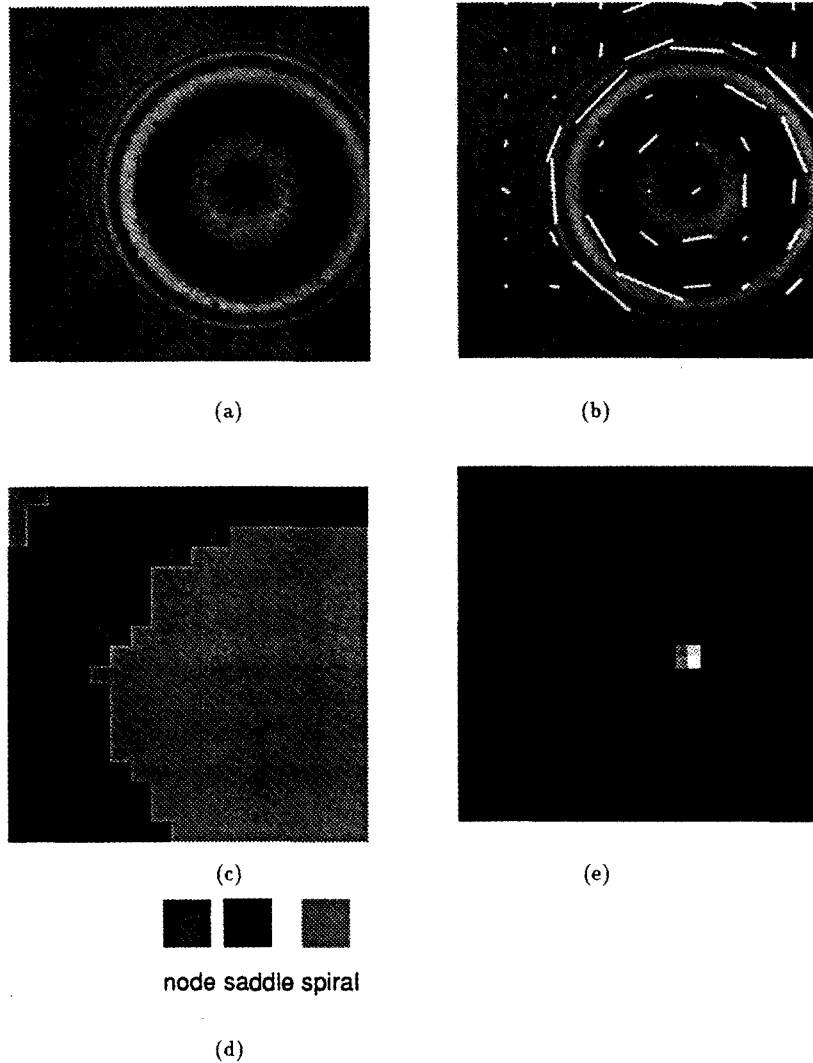

(a)

(b)

(c)

(e)

node saddle spiral

(d)

Fig. 5. (a) The original image of the resist gel defect. (b) The orientation field overlayed on the original image in the form of white segments. The length of each oriented segment is proportional to the coherence. (c) The segmented image. The different types of phase portraits possible have been coded. Note that the areas around the defect are classified as spiral regions. (d) Shading key for phase portraits. (e) Map of spiral fixed points.

```
Description of given image:
 Spiral fixed points located
 at following points:-
 Row = 14, col = 17;

 Values of A and B matrices are:-
 A  =  0         1
       -1.0402   -0.0017

 B  =  -0.3111  0.4165
      at  (14, 17)
                              a
```
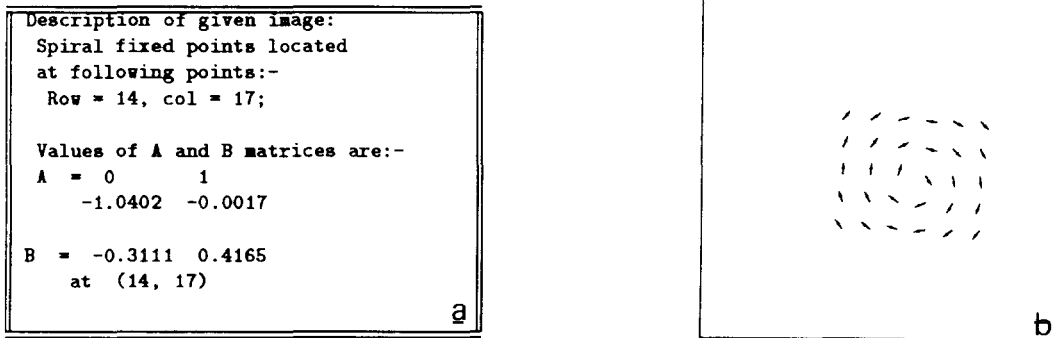
Fig. 6. (a) Symbolic description of the input image. (b) Reconstructed image, based on this symbolic description. This corresponds to the original image in fig. 5. Observe that the salient feature of the original image, namely the concentric circles of the texture, has been captured in the reconstructed image.
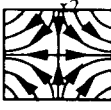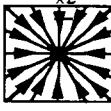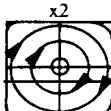
CASE	JORDAN FORM	TYPE OF PHASE PORTRAIT	APPEARANCE OF PHASE PORTRAIT
1) Real distinct eigenvalues $\lambda 1, \lambda 2$ with $\lambda 1 > \lambda 2$	(a) $\begin{bmatrix} \lambda 1 & 0 \\ 0 & \lambda 2 \end{bmatrix}$ $\lambda 1$ and $\lambda 2$ have the same sign	NODE	
	(b) $\begin{bmatrix} \lambda 1 & 0 \\ 0 & \lambda 2 \end{bmatrix}$ $\lambda 1$ and $\lambda 2$ have opposite sign	SADDLE	
2) Equal eigenvalues $\lambda 1 = \lambda 2 = \lambda 0$	(a) $\begin{bmatrix} \lambda 0 & 0 \\ 0 & \lambda 0 \end{bmatrix}$	STAR-NODE	
	(b) $\begin{bmatrix} \lambda 0 & 1 \\ 0 & \lambda 0 \end{bmatrix}$	IMPROPER NODE	
3) Complex eigenvalues $\lambda 1 = \alpha + \iota\beta$ $\lambda 2 = \alpha - \iota\beta$ $\alpha = \frac{1}{2} tr(A)$ $\beta = \frac{1}{2}\sqrt{-\Delta}$	$\begin{bmatrix} \alpha & -\beta \\ \beta & \alpha \end{bmatrix}$ (a) $\alpha = 0$	CENTER	
	(b) $\alpha \neq 0$	SPIRAL	

Fig. 7. Classification of different phase portraits based on the nature of the eigenvalues and the associated Jordan forms.

but is displayed in a sampled form in order to avoid clutter.

In fig. 5b, the orientation field is overlayed on the original image to aid comparison. The orientation at each point is represented by means of a line segment, whose direction corresponds to the dominant local orientation, and whose length is proportional to the coherence. Observe that the segments capture the orientation of the texture at each point, and orient themselves along the direction of dominant orientation.

Fig. 5c shows the initially segmented flow image. Segmentation is performed into the following classes: nodes, spirals, and saddles (this is the smallest number of equivalence classes). The segmented regions are gray-level coded, according to the scheme shown in fig. 5d.

Fig. 5e shows the spiral fixed point map. The map is printed such that the likelihood of a map point being a fixed point is proportional to the intensity at that point. The location of the fixed point agrees with the nature of the original defect image.

Reconstruction of the resist gel defect

The symbolic description of the image is automatically generated from the program as shown in fig. 6a. Fig. 6b shows the reconstructed flow image based on values for *A* and *b* at the saddle fixed points.

4.2. Application to semiconductor defect identification

In section 1 we had mentioned problems faced by inspection personnel in trying to describe defects accurately. Based on the theory and results presented in this paper, we are now in a position

Table 1
A scientific terminology for describing some defects arising in semiconductor wafer processing

Currently used jargon	Equivalent scientific term
Star-bust	Star node
Worm hole	Center
Speedboat	Section of a saddle
Hillock	Surface with high fractal dimension

to give a much more scientific scheme to describe and classify the same defects. Table 1 illustrates new terms for the jargon currently being used. The appropriateness of the new scheme can be readily seen by comparing fig. 1 which shows the appearance of the defects, with fig. 7, which shows linear phase portraits in the 2D case.

5. Conclusion

In this paper we presented a novel method to classify textural defects arising in semiconductor wafer inspection. This method involves a taxonomy for textures. We have provided the qualitative symbols that form the taxonomy and also computational techniques to extract these symbols.

We presented results of applying this technique to real texture images of semiconductor wafers.

Acknowledgements

References

[1] A.R. Rao and R. Jain, in: Vision 88 (Society of Manufacturing Engineers, Detroit, MI, 1988).
[2] R. Conners, C.W. McMillin, K. Lin and R.E. Vasquez-Espinosa, IEEE Trans. Pattern Analysis and Machine Intelligence 5 (1983) 573.
[3] E.S. Meieran, P.A. Flinee and J.R. Carruthers, Proc. IEEE 75 (1987) 908.
[4] J.J. Gagnepain and C. Roques-Carmes, Wear 109 (1986) 119.
[5] A. Pentland, IEEE Trans. Pattern Analysis and Machine Intelligence 6 (1984) 661.
[6] R. Jain, A.R. Rao, A. Kayaalp and C. Cole, in: Machine

Vision for Inspection and Measurement, Ed. H. Freeman (Academic Press, New York, 1989).

[7] A.R. Rao and B.G. Schunck, in: Proc. Conf. on Computer Vision and Pattern Recognition (IEEE, New York, 1989).

[8] D.K. Arrowsmith and C.M. Place, Ordinary Differential Equations: A Qualitative Approach with Applications (Chapman and Hall, London, 1982).

[9] S. Lefschetz, Differential Equations: Geometric Theory (Interscience, New York, 1963).

[10] A.R. Rao, A Taxonomy for Texture Description and Identification (Springer, Berlin, 1990).

[11] D.J. Elliott, Integrated Circuit Mask Technology (Mc-Graw-Hill, New York, 1985).